ELSEVIER

International Journal of Heat and Fluid Flow 21 (2000) 65–73

International Journal of HEAT AND FLUID FLOW

www.elsevier.com/locate/ijhff

Thermoconvective instabilities in a narrow horizontal air-filled annulus

Gilles Desrayaud [b], Guy Lauriat [a,*], Pierre Cadiou [a]

[a] *Université de Marne-la-Vallée, Cité Descartes, Bât. Lavoisier, Champs-sur-Marne, 77454 Marne-la-Vallée Cedex 2, France*
[b] *INSSET, Université de Picardie, 48 rue Raspail, B.P. 422, 02109 Saint-Quentin, France*

Received 30 October 1998; accepted 3 May 1999

Abstract

This paper reports a numerical investigation of natural convection flows between horizontal concentric annuli with the inner cylinder isothermally heated. Thermal and hydrodynamic instabilities for air-filled annuli of small radius ratios are discussed. At fairly low Rayleigh numbers ($Ra \leqslant 3000$), thermal instabilities develop at the upper part of the annulus as steady cells. The results show the existence of an imperfect bifurcation, which could explain the discrepancies between the solutions reported previously in the literature. Locations of the bifurcation points are determined numerically for various radius ratios. At higher Rayleigh numbers, unsteady hydrodynamic instabilities are demonstrated in the vertical portions of an annulus with a radius ratio $R = 1.14$. It is also shown that a reverse transition from multicellular to unicellular base flow patterns occurs when further increasing the Rayleigh number.

Keywords: Air-filled annulus; Natural convection; Thermal and hydrodynamic instabilities

Notation

g	acceleration due to gravity
Gr	Grashof number ($Gr = Ra/Pr$)
e'	gap width ($e' = r'_o - r'_i$)
Pr	Prandtl number ($Pr = \nu/\alpha$)
r	dimensionless radial coordinate ($r = r'/e'$)
r_i	dimensionless inner cylinder radius ($r_i = r'_i/e'$)
r_o	dimensionless outer cylinder radius ($r_o = r'_o/e'$)
R	radius ratio ($R = r'_o/r'_i$)
Ra	Rayleigh number $Ra = g\,\beta\,e'^3\Delta T/\alpha\nu$)
T	dimensionless time ($t = \alpha\,t'/e'^2$)
T_m	mean temperature ($T_m = 0.5(T_i + T_o)$)
u, v	radial and azimutal velocity
Greek	
α	thermal diffusivity
β	coefficient of thermal expansion
ν	kinematic viscosity
θ	angular coordinate measured from downward vertical
Θ	dimensionless temperature ($\Theta = (T - T_m)/\Delta T$)
ΔT	temperature difference ($\Delta T = T_i - T_o$)
Superscript	
$'$	dimensional variables
Subscripts	
i	inner cylinder
o	outer cylinder

1. Introduction

Natural convection between horizontal isothermal concentric cylinders has been widely studied theoretically and experimentally over the past three decades because of the importance of this subject in industrial problems, such as transmission cable cooling systems, latent energy storage systems, nuclear reactor design, etc. From a theoretical point of view, natural convection in horizontal annuli has been one of the focuses of research in heat transfer on account of the large variety of flow structures encountered in this configuration according to the value of the radius ratio. For example, two-dimensional Rayleigh–Bénard like solutions are shown at the top annulus region for small annular gap while oscillating thermal plumes are seen to develop for large radius ratios. The computations carried out in the present study deal with the small radius ratio configuration for which large discrepancies are reported in the literature, especially about the flow structure at the low Rayleigh numbers just above the first bifurcation point.

* Corresponding author.
E-mail address: lauriat@univ-mlv.fr (G. Lauriat).

0142-727X/00/$ - see front matter
PII: S0142-727X(99)00048-X

From their experimental work, Powe et al. (1969) depicted flow regime transitions for air-filled annuli and were the first to present a chart for the prediction of the nature of the flow according to the Rayleigh number and radius ratio. This chart shows the limit between the base flow and the two- or three-dimensional flow patterns, stationary or oscillatory, which follow the named pseudo-conduction regime. This basic flow field consists of two crescent-shaped cells, symmetrical with respect to the vertical plane containing the axes of the cylinders. In each of the two annular half spaces, the fluid follows an upward stream along the hot inner cylinder and finally reaches the top of the annular space. The fluid goes then downwards along the cold cylinder and reaches the almost quiescent bottom portion of the annulus. At low Rayleigh number, conduction is the major mode of heat transfer between the hot and cold cylinders. As the Rayleigh number is increased, the center of rotation of the main cells moves upward and a thermal plume starts to form at the upper part of the annulus with an impingement region at the outer cylinder. The shape of the isotherms shows that the largest part of the heat convected within the annulus is extracted from the lower part of the inner cylinder. At small radius ratios ($R \leqslant 1.20$), the flow becomes multicellular while remaining two-dimensional when increasing the Rayleigh number. In the thermally unstable regime, two-dimensional cells aligned along the axis of the cylinders form at the top of the annulus, just between the two main cells of the base flow. For higher radius ratios ($1.24 \leqslant R \leqslant 1.71$), a three-dimensional flow develops after the first bifurcation, a spiral motion being superimposed on the base flow which is still in the shape of a crescent. A vertical cut in the axial direction shows a flow structure of Rayleigh–Bénard type at the top of annular cavity. Lastly, an oscillating three-dimensional thermal plume is observed in the higher part of annular space when $R \geqslant 2$.

In the case of an annular cavity of small radius ratio ($R \leqslant 1.20$), the discrepancies found between the results reported in the literature are both on the flow patterns and critical Rayleigh numbers corresponding to the bifurcation points. Powe et al. (1969) showed experimentally that cells form within the upper part of the annulus when $4100<\mathrm{Ra}<4900$. This two-dimensional structure of the flow was then confirmed numerically by Powe et al. (1971), Rao et al. (1985), Fant et al. (1989) and Kim and Ro (1994). Rao et al. (1985) simulated only one stationary multicellular flow having four secondary cells at the annulus top region for $R = 1.175$ and $\mathrm{Ra} = 4000$, although several initial conditions were used. They also showed that the flow comes to oscillate at moderate Rayleigh numbers ($\mathrm{Ra} \leqslant 50\,000$) in such a way that the top cells periodically swing right and left. Fant et al. (1989) calculated a multicellular flow with two secondary cells for $R = 1.20$ and $\mathrm{Ra} \geqslant 2841$ and evidenced a hysteresis phenomenon in the range $2570 \leqslant \mathrm{Ra} \leqslant 2841$. Since the two cells obtained were counter-rotating, a downward velocity in the vertical plane of symmetry and an inverted thermal plume resulted at the top annulus region. For the same radius ratio, Kim and Ro (1994) calculated two stable flow structures characterized by different numbers of secondary cells (2 or 4). These two solutions were calculated using different initial conditions. Two critical Rayleigh numbers are reported in Kim and Ro (1994), one for each branch of the bifurcation phenomenon. For $R = 2^{0.5}$, Cheddadi et al. (1992) obtained two secondary cells but at $\mathrm{Ra} \geqslant 3250$ only, and by using a perturbed temperature distribution as an initial condition. Without initial disturbance, the base-flow pattern was found to be stable up to $\mathrm{Ra} = 7000$. Moreover, they did not report hysteresis phenomena. Finally, the recent numerical study of Barbosa-Mota and Saatdjian (1994) dealing with a porous-filled annulus showed the existence of a critical radius ratio ($R = 1.7$) beyond which hysteresis phenomena can exist. Their results show also that the critical Darcy-modified Rayleigh number tends towards $4\pi^2$ when the radius ratio tends towards unity. This result supports the analogy between natural convection within narrow horizontal annuli and horizontal layers heated from below.

To our best knowledge Fant et al. (1989, 1990) were the only ones to describe the appearance of longitudinal rolls within the main crescent-shaped cells, but in the limiting case of zero Prandtl-number fluids. These instabilities are hydrodynamic in nature. It was shown that the number of cells is a strong function of the radius ratio. For example, four or five cells form in each vertical part of the annulus beyond a critical Rayleigh number at $R = 1.09$, the cell number oscillating between 4 and 5 during one period.

In the present study, either 2D steady or transient investigations are performed to simulate natural convection within the annuli of small radius ratio ($R \leqslant 1.20$). The reasons for the above-mentioned discrepancies are explained through the discussion of the numerical results. To show the dependence of the flow pattern on the initial condition, computations are first carried out by gradually increasing Ra from a motionless isothermal state. Secondly, flow patterns at $\mathrm{Ra} = 3000$ are obtained by starting from a motionless state with a perturbed pure conductive temperature distribution, the next calculations being continued by slightly decreasing Ra until the pseudo-conduction regime is recovered. Finally, time-periodic solutions are shown to appear at moderate Ra, followed by a reverse transition to a unicellular crescent-shaped base flow when increasing further Ra.

Recently, after the work reported in this paper was completed, an investigation dealing with the same problem but at low Prandtl numbers ($\mathrm{Pr} \leqslant 0.3$) for an annulus of aspect ratio $R = 1.167$ was published by Yoo (1998). He found that the Prandtl number has a strong influence upon the type of instability of the conduction dominated flow. For $\mathrm{Pr} \leqslant 0.2$, only hydrodynamic instabilities set in as steady or oscillatory rotating cells in the vertical section of the annulus as in a vertical slot. For $\mathrm{Pr} = 0.3$, the first instability is thermal in its origin and is formed at the top of the annulus as steady counter-rotating cells. When increasing the Rayleigh number, the steady multicellulear flow undergoes hydrodynamic instabilities which consist of multiple oscillatory rotating cells in the vertical section. The results obtained by Yoo (1998) for a $\mathrm{Pr} = 0.3$ are consistent with those presented here.

2. Equations and numerical procedure

Fig. 1 illustrates schematically the physical problem of natural convection within a horizontal annulus made of two concentric isothermal cylinders. The inner cylinder of radius r_i is heated at uniform temperature T_i whereas the outer cylinder of radius r_o is at a lower temperature, T_o. The mathematical formulation of the problem is written in cylindrical coordinates with the origin at the center of the inner cylinder. The angular coordinate θ is measured from the vertical, positively in the trigonometrical direction. The flow is assumed to be incompressible, laminar, Newtonian and two-dimensional. The thermophysical properties of the fluid are taken at the average temperature, T_m, except the density in the buoyancy term which is a linear function of the temperature gradient. The Boussinesq-approximated Navier–Stokes equations and energy equation with negligible viscous dissipation are used to determine the buoyancy-induced flow field. These equations written in dimensionless form are given by

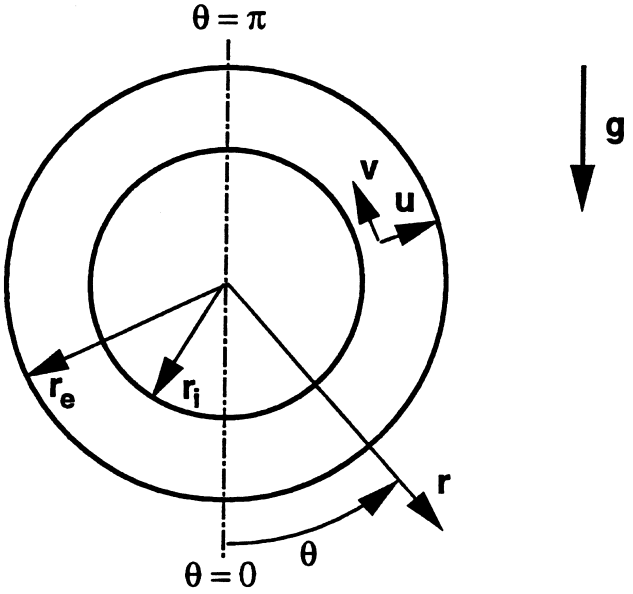

Fig. 1. Flow geometry and coordinate system.

$$\nabla \cdot \mathbf{U} = 0, \tag{1}$$

$$\frac{\partial \mathbf{U}}{\partial t} + (\mathbf{U} \cdot \nabla)\mathbf{U} = -\nabla p + \mathrm{Pr} \cdot \Delta \mathbf{U} + \mathrm{Ra} \cdot \mathrm{Pr} \cdot \Theta \cdot \mathbf{j}, \tag{2}$$

$$\frac{\partial \Theta}{\partial t} + (\mathbf{U} \cdot \nabla)\Theta = \Delta \Theta. \tag{3}$$

The problem depends on one geometrical parameter, the radius ratio R, and two dimensionless numbers, the Rayleigh number, Ra, which is built on the spacing between cylinders, and the Prandtl number, Pr. In the present paper, all the calculations were carried out for $\mathrm{Pr} = 0.71$ (air).

The boundary conditions at the inner and outer cylinders are as follows:

$$r = r_\mathrm{i} \text{ and } 0^\circ \leqslant \theta \leqslant 2\pi : u = v = 0 \text{ and } \Theta = +0.5, \tag{4}$$

$$r = r_\mathrm{o} \text{ and } 0^\circ \leqslant \theta \leqslant 2\pi : u = v = 0 \text{ and } \Theta = -0.5. \tag{5}$$

The local Nusselt number is given by

$$\mathrm{Nu}(r, \theta) = \ln R (u\Theta - \partial\Theta/\partial r)\, r. \tag{6}$$

The mean Nusselt numbers on the inner and outer cylinders are calculated by averaging the local Nusselt number on the area of the cylinders:

$$\overline{\mathrm{Nu}_\mathrm{i}} = -\frac{r_\mathrm{i} \ln R}{2\pi} \int_0^{2\pi} \left(\frac{\partial \Theta}{\partial r} \right)_{r=r_\mathrm{i}} \mathrm{d}\theta, \tag{7}$$

$$\overline{\mathrm{Nu}_\mathrm{o}} = -\frac{r_\mathrm{o} \ln R}{2\pi} \int_0^{2\pi} \left(\frac{\partial \Theta}{\partial r} \right)_{r=r_\mathrm{o}} \mathrm{d}\theta. \tag{8}$$

At steady state, these mean Nusselt numbers should be equal. This condition can be considered as a physical criterion for checking the accuracy of the numerical solutions.

The governing equations were discretized using a finite volume method. The SIMPLER algorithm was used to solve the velocity–pressure coupling and a centered approximation was employed to discretize the convective terms. All the equations were solved in transient form with a semi-implicit scheme for temporal integration (ADI method). The resulting tridiagonal matrix systems were solved by using a vectorized version of a direct matrix solver (Thomas algorithm).

On account of the results reported by Powe et al. (1971), Cheddadi et al. (1992), Kim and Ro (1994) and Cadiou et al. (1995) and of the numerous computations carried out in the present study, it can be concluded that the calculation may be made on half annulus at low Rayleigh numbers (at which the solution is stationary and symmetrical) whereas the whole annulus must be considered for higher Rayleigh numbers at which oscillations of the problem variables may occur within the flow field.

When calculations are carried out on a half-cavity, the conditions of symmetry are as follows

$$\text{at } \theta = 0 \text{ and } \theta = \pi,\ r_\mathrm{i} \leqslant r \leqslant r_\mathrm{o} : v = 0 \text{ and } \frac{\partial u}{\partial \theta} = \frac{\partial \Theta}{\partial \theta} = 0. \tag{6}$$

For a whole cavity, boundary conditions of periodic type were applied at $\theta = 0$ and 2π. It consists in using the solutions calculated at a previous radial sweeping as the boundary conditions at the angular sweeping of the ADI procedure.

Grid refinement studies were conducted for several radius ratios. The results are reported in Tables 1 and 2 for $R = 1.2$. The numbers of points in the radial and angular directions (on a half-cavity) are denoted n_r and n_θ. The values of the various variables obtained on the same grids using a finite element code (TRIO-EF developed at the French Atomic Energy Center in Saclay by Magnaud et al., 1997) are given in brackets. It should be noted that calculations were not made for the finest grid because the CPU-time becomes prohibitively large when running TRIO-EF on a workstation.

Comparisons between mean Nusselt numbers and local values, i.e. the norm of the maximum velocity, are given in Table 1 for various grid sizes at $\mathrm{Ra} = 3000$. The Rayleigh numbers corresponding to a transition from the base flow to a multicellular flow are reported in Table 2. The results between brackets are those obtained using TRIO-EF. The same multicellular patterns were obtained using both codes (Cadiou, 1997). In addition, Tables 1 and 2 show a very good agreement between the local, average and transitional values obtained.

The result of this grid refinement study was to select uniform meshes both in radial and angular directions having 19×110 nodes for half-annulus computations conducted at low Rayleigh numbers ($\mathrm{Ra} < 5000$), and 31×240 nodes for possibly oscillating flows ($5000 < \mathrm{Ra} < 50\,000$) at which the full annulus was discretized. These grid systems were considered as a good compromise between accuracy of the solutions and determination of the bifurcation points, and CPU-time. All the

Table 1
Mean Nusselt number and maximums of the mean velocity for various grid systems ($R = 1.20$, $\mathrm{Ra} = 3000$, $\mathrm{Pr} = 0.71$)[a]

$n_r - n_\theta$	13–74	19–110	25–146	41–246
$\overline{\mathrm{Nu}}$	1.134	1.127	1.124	1.122
	(1.109)	(1.116)	(1.118)	(–)
$\max \sqrt{u^2 + v^2}$	23.37	23.86	24.03	24.06
	(23.27)	(23.78)	(23.92)	(–)

[a] The values in parenthesis are for the finite element code.

Table 2
Rayleigh numbers at which multicellular structures appear ($R = 1.20$, $\mathrm{Pr} = 0.71$)[a]

$n_\mathrm{r} - n_\theta$	19–110	25–146	35–202
Ra	1880	1915	1925
	(1950)	(1920)	(–)

[a] The values in parenthesis are for the finite element code.

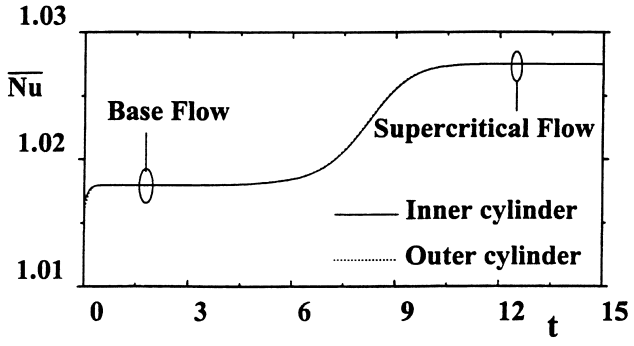

Fig. 2. Time evolution of the mean Nusselt numbers at $Ra = 2000$, $R = 1.20$ and $Pr = 0.71$ (initial solution $Ra = 1900$).

finite volume calculations were carried out on a CRAY C90 with a 400 Mflops-speed on average.

It should be underlined that an accurate localization of the thresholds of transition between unicellular and multicellular flows is highly CPU-time consuming. As an example, Fig. 2 shows the time evolution of the average Nusselt number for $Ra = 2000$, the initial solution being the computed stationary solution at $Ra = 1900$. From time $t = 1$ to 5, the Nusselt number does not vary within seven decimals. The choice of a too weak convergence stopping criterion would have led to end the calculations. The transition occurs at about $t = 7$, i.e. 14 000 iterations with a time increment $\Delta t = 5 \times 10^{-4}$. The abrupt changes in Nu means that the solution evolves then to a multicellular flow. Such a behavior was noticed by Rao et al. (1985). This result shows that the use of convergence criteria, whatever they are, when searching thresholds of flow transition is inappropriate as demonstrated by Desrayaud and Lauriat (1991). It seems better to fix a total number of time steps, although this procedure leads obviously to very long CPU-times when conducting a parametric study.

3. Results and discussion

3.1. Flow patterns at low Rayleigh numbers

Natural convection flows in horizontal annuli with heated inner cylinder merge with Rayleigh–Bénard flows between two infinite parallel plates as the radius ratio tends towards unity. It should be noted that this limit is highly difficult to reach numerically with the code used in the present work owing to the drastic increase in CPU-time as $R \to 1$. For the Rayleigh–Bénard problem the fluid is initially at rest because the stabilizing effect of the viscous forces is higher than the destabilizing effect of buoyancy. For a fluid layer of infinite horizontal extension, this state is modified above $Ra_c = 1708$ and the multicellular flow patterns and types of bifurcations occurring then were considered in a number of works (see for example Bergé et al., 1984). In the finite box configuration, the flow pattern evolves towards two possible stable states through a pitchfork bifurcation. Longitudinal cells of horizontal axis are formed between the two horizontal plates with an equal probability of rotating in clockwise direction or in the opposite. This feature evidences that there exist two symmetrical stable branches of bifurcation. However, it should be noted that while one of the two bifurcation branches is naturally followed when increasing progressively the Rayleigh number, the other branch cannot be reached in numerical experiments without superimposing small perturbations to the pure conduction temperature field used as initial condition.

For a horizontal air-filled annulus, the curvature of the surfaces (or radius ratio) can be considered as an external perturbation that controls the secondary cell generation. Indeed, curvature has a strong effect on the two-dimensional unicellular base flow, named the pseudo-conduction regime, which develops within each half of the annulus at low Rayleigh number with an upward velocity in the vertical center plane. This flow pattern exists as soon as the temperatures of the cylinders differ. It should be noted that a temperature gradient co-linear and opposite to the gravity vector exists at $\theta = \pi$ and temperature gradients perpendicular to gravity exist at $\theta = \pi/2$ and $3\pi/2$. Therefore, onset of the Rayleigh–Bénard type flow is possible at $\theta = \pi$ while a fluid motion is created around $\theta = \pi/2$ and $3\pi/2$, whatever the temperature difference. One can thus expect to observe thermal instabilities of the Rayleigh–Bénard type at the top of the annulus provided that the radius ratio is small enough, and also hydrodynamic instabilities like in vertical slots filled with low Prandtl number fluids (Lee and Korpela, 1983).

In the present study, it was necessary to work with two procedures similar to those used for the Rayleigh–Bénard problem in order to follow the bifurcation branches. These branches may be displayed through plots of variations of field variables as a function of Ra or variations of the Nusselt number. The first procedure consisted in gradually increasing the Rayleigh number, an isothermal and motionless fluid being used as the initial condition when solving the governing equations at the lowest Rayleigh number considered. The continuous branch was then obtained from increases in Ra and the transition from the unicellular base flow to a multicellular flow occurs at a Rayleigh number named in what follows *transitional Rayleigh number*. The second branch can only be found by disturbing the flow field, i.e. either by superimposing thermal perturbations to an initial state of pure conduction (Cheddadi et al., 1992), or by abruptly increasing the Rayleigh number when starting from an isothermal motionless fluid. However, it should be noted that an abrupt increase in Ra produces a solution located on the second branch only if the Ra-value is far from the critical value and for large enough radius ratios ($R \geqslant 1.20$). On account of the small radius ratios investigated in the present study, it was necessary to use a perturbed pure conduction solution together with an abrupt change in Ra in order to reach the second branch of bifurcation. Thus, this branch was followed by decreasing Ra and appears to be the isolated branch of an imperfect bifurcation. The lowest value of the Rayleigh number found on this isolated branch is called in the following the *critical Rayleigh number*.

3.1.1. Case $R = 1.08$

Since our numerical simulations were aimed at simulating secondary cells, the results are first discussed for $R = 1.08$ because a large number of thermal cells may develop at the upper part of the annulus. The onset of secondary cells is indeed inhibited when R is far from unity. Therefore, the study of the process of formation or merging of secondary cells is easier when the computations are carried out for annuli of small radius ratios. However, all of the isothermal patterns and streamlines shown in the present paper were plotted for an annulus with $R = 2$, whatever the current value of R is (except in Fig. 6), in order to improve the graphical representations.

When using the first procedure, the results showed that the pseudo-conduction regime persisted up to $Ra = 1755$ (Fig. 3a). Around $Ra = 1785$, the two crescent-shaped cells of the base flow divided at the top the annulus and onset of a small secondary cell within each half-annulus is evidenced (Fig. 3b). These cells are co-rotating with the main cells. When following the continuous branch, the velocity at the symmetry plane

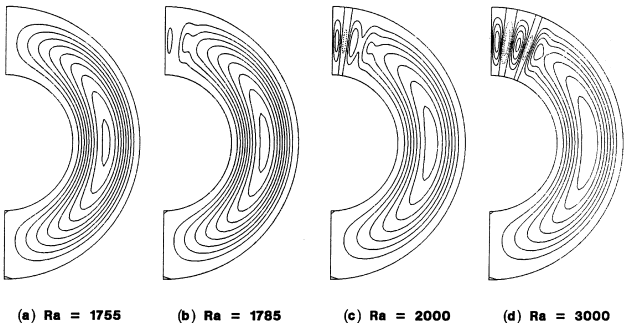

Fig. 3. Streamlines for the stationary regime obtained through regular increases in Ra ($R = 1.08$, $\mathrm{Pr} = 0.71$).

($\theta = \pi$) is upward. In what follows, the branch with the upward velocity at $\theta = \pi$ will be thus named U-branch. The top cells are difficult to detect from the isothermal patterns and streamlines at Ra-values very close to the threshold of transition. On the other hand, plots of the local Nusselt number allow to easily detect their onset provided that a stationary multicellular state exists. Fig. 4 shows clearly the effect of the top cell on the local Nusselt number distributions at $\mathrm{Ra} = 1785$. It should be noted that to simulate such a flow field requires a large integration time. Fig. 3c ($\mathrm{Ra} = 2000$) was prepared to exemplify the beginning of a cycle of formation of the thermal cells. At the top of the main cell, a secondary cell is almost formed through a separation process from the crescent base flow. When separation is ended this cell is co-rotating with the base flow. It is rather surprising to observe the existence of a flow structure having co-rotating cells. Within the inter-cells region, large shear stresses occur. As a result, this flow structure cannot persist and the emergence of an additional cell is observed when increasing Ra: a stagnation zone appears as the top cell strengthens and a counter-rotating cell starts to rise as soon as the extent of this stagnation zone is large enough. For example, at $\mathrm{Ra} = 3000$ (Fig. 3d) the cell which was forming at $\mathrm{Ra} = 2000$ (Fig. 3c) is fully separated from the main cell and a counter-rotating cell (plotted in dashed lines) has appeared between these cells. Further increases in Ra lead to a third separation of the main cell.

From the computations carried out in this work for annuli of small radius ratios ($1.04 \leqslant R \leqslant 1.20$), it has been found that the cycle of formation of the cells systematically proceeds as follows: when all of the cells are counter-rotating, a new cell rises by separation from the base flow. This cell is co-rotating with the main cell. By increasing Ra the extent of the stagnation zone between these two co-rotating cells makes the onset of a counter-rotating cell possible. Then the cycle starts again until the curvature of the annulus prevents the formation of an additional cell. This is why the number of cells decreases when the radius ratio increases.

It should be noted that the above-mentioned process of cell formation is inverted when decreasing Ra. For the radius ratio considered here, the transition towards the unicellular base flow (pseudo-conduction regime) occurs at almost the same Rayleigh number as the transitional Ra calculated by increasing Ra.

By starting the computations from a motionless and isothermal state ($\Theta = -0.5$) as an initial condition, an abrupt change in Rayleigh number up to $\mathrm{Ra} = 3000$ was not enough to simulate a solution located on the isolated branch for $R = 1.08$. Therefore, it was necessary to start the computations by using a theoretical model consisting in a motionless fluid in which the temperature field was that of a pure conduction solution, disturbed such as (Cheddadi et al., 1992)

$$\Theta(r,\theta) = 0.5 - \frac{1}{\ln R}\ln\left[(R-1)\,r+1\right] + \alpha\sin\left[\frac{\pi}{\ln R}\ln\left[(R-1)\,r+1\right]\right]\cos\eta\theta,$$

where α is the amplification factor and η is the wave number. When choosing $\alpha = 0.02$ and $\eta = 16$, the isolated branch of bifurcation is then reached at $\mathrm{Ra} = 3000$. The downward velocity along the vertical axis in the upper part of the annulus characterizes this branch (uppermost cell plotted in dashed lines in Fig. 5a). Therefore, the branch with a downward velocity at $\theta = \pi$ will be named D-branch. Three counter-rotating top cells develop then within each half-annulus. It can also be seen that a fourth cell is almost detached from the base flow and would give rise to a cell co-rotating with the main cell at a slightly higher Ra. On the other hand, when the Rayleigh number is decreased to $\mathrm{Ra} = 1980$ (Fig. 5b), this cell merges and the base flow extends towards the top region of the annulus. Consequently, the flow rate within the secondary cell adjacent to the base flow is damped out until its ultimate disappearance. The result is that the cell, which becomes the nearest to the base flow, is then co-rotating. Further decrease in Ra leads to a breaking-up of one more cell through a continuously crunching process by the main cell. It should be noted that the velocity at the top of the symmetry plane ($\theta = \pi$) is downward whatever Ra is. Finally, the flow field exhibits a monocellular pattern for Ra within the range $1785 < \mathrm{Ra} < 1755$ (Fig. 5d).

On the D-branch, the mechanism of formation (increase in Ra) or merging (decrease in Ra) of the cells within the upper

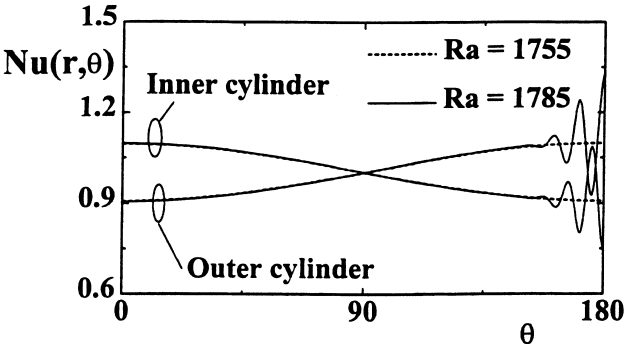

Fig. 4. Angular variations of the mean Nusselt numbers on the isothermal cylinders ($R = 1.08$, $\mathrm{Pr} = 0.71$).

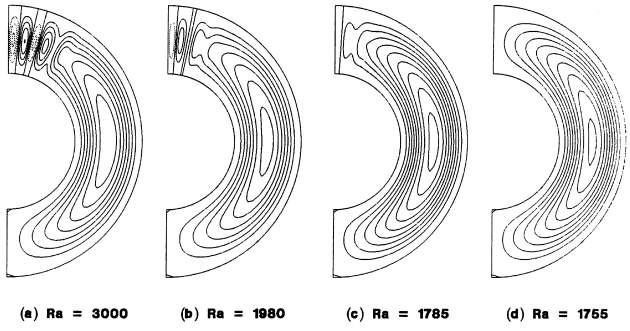

Fig. 5. Streamlines for the stationary regime obtained through decreases in Ra ($R = 1.08$, $\mathrm{Pr} = 0.71$).

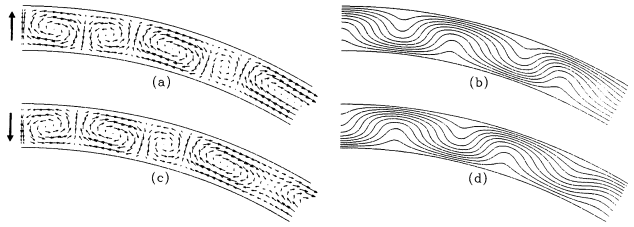

Fig. 6. Velocity field and isotherms on both branches of the bifurcation at $Ra = 3000$: U-branch (a,b), D-branch (c,d) ($R = 1.08$, $Pr = 0.71$).

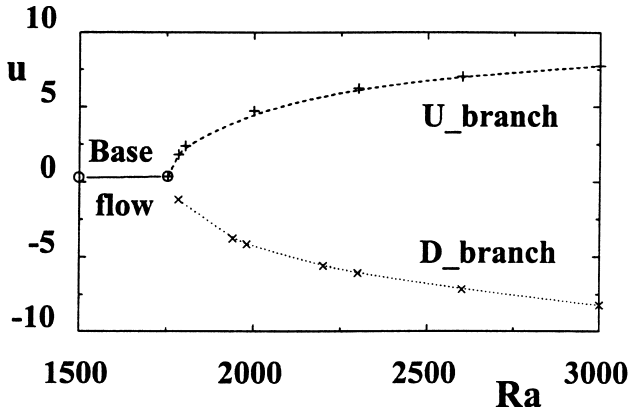

Fig. 7. Bifurcation map of the radial component of velocity at $r = 0.5(r_i + r_o)$ and $\theta = \pi$ ($R = 1.08$, $Pr = 0.71$).

part of the annulus is similar to the one that has been described for the U-branch. On the other hand, the velocity in the symmetry plane at the annulus top region is upward for solutions located on the U-branch and downward for those on the D-branch. Fig. 6 which shows the isotherms at $Ra = 3000$ exemplifies this difference. As can be seen, a thermal plume is formed at the vertical plane of symmetry (Fig. 6b) for the solution on the U-branch while a reversed thermal plume develops if the solution is on the D-branch (Fig. 6d). This feature characterizes also the two branches of the bifurcation. Fant et al. (1989) and Yoo (1998) had already reported the existence of a thermal plume reversed or not but did not give any reason for it. Only one branch (the U-branch in the present case) can be followed continuously, i.e. by increasing or decreasing Ra, through the threshold at which onset of multicellular flow occurs at the annulus top. The other branch shows a discontinuity. The D-branch can indeed be followed only by decreasing Ra down to a critical value below which the pseudo-conductive regime is obtained anew. It seems that the pitchfork bifurcation found in the Rayleigh–Bénard problem (i.e. $R = 1$) degenerates into an imperfect bifurcation under the effect of the curvature which breaks the $z \to -z$ symmetry of the velocity field. This dissymmetry breaks the Rayleigh–Bénard solutions which bifurcate at the double point of the pitchfork bifurcation into two supercritical isolated solutions. These solutions correspond to the U- and D-branches. Furthermore, the hysteresis phenomenon, which is one of the main feature of a transcritical bifurcation (an another degeneracy of the pitchfork bifurcation), has never been detected whatever the radius ratio was. Calculations carried out for higher radius ratios (up to $R = 1.20$ at which the threshold is within the interval [1900,1920]) did not allow us to show evidence of a hysteresis phenomenon. Fig. 7 exemplifies this finding by showing the variations of the radial velocity at $\theta = \pi$ and at the middle of the annulus gap as a function of Ra. The continuous and the isolated branches of the imperfect bifurcation are drawn. The transitional Ra for the onset of multicellular flow at the top of the annulus ranges from 1720 to 1750 when determined by increasing Ra. By decreasing Ra, the critical point of bifurcation was found in the same range, i.e. $1750 \leqslant Ra_c \leqslant 1720$. On the D-branch, the evolution of the velocity amplitude at point ($r = 0.5(r_i + r_o)$, $\theta = \pi$) follows a law of the type $\{(Ra - Ra_c)/Ra_c\}^{0.5}$ while no precise law was found on the U-branch. These results corroborate the existence of an imperfect bifurcation.

3.1.2. Transitional values and correlation

In the present study, five radius ratios were considered: $R = 1.04$, 1.08, 1.12, 1.16 and 1.20. From the purely numerical determination of the transitional Rayleigh numbers, the following correlation giving Ra_T as a function of R was obtained using a linear regression procedure

$$Ra_T(R) = 552 + 1150\ R. \tag{10}$$

The maximum deviation of this correlation from the numerical data is within 0.6% and it is in very good agreement with the results reported by Cadiou et al. (1995) by using a finite element method. The critical value obtained by extrapolation for $R = 1$ is very close to $Ra_c = 1708$. The critical Ra given by Kim and Ro (1994) for $1.2 \leqslant R \leqslant 1.6$ are reported in Table 3. It can be seen that the relative errors between their values and those based on Eq. (10) are within 2%, even for the highest radius ratio at which extrapolation was used. It should also be noted that the present transitional values are also in good agreement with those reported in the flow regime chart of Powe et al. (1969). In the present work, computations were not carried out for radius ratios greater than 1.20 since a transition to 3D-flows has been revealed by experiments (Powe et al., 1969).

Fig. 8 displays the variations of the mean Nusselt numbers on the two branches of bifurcation as a function of Ra for the five radius ratios considered. For each of the radius ratios, the number of cells increases with Ra. At a fixed value of Ra, the number of cells increases as R decreases. For example, eight cells are simulated for $R = 1.04$ at $Ra = 3000$ while they are only one or two cells for $R = 1.16$ and 1.20 according to the location of the solution on the branches. The number of secondary cells observed on the two branches at $Ra = 3000$ is reported between brackets in Fig. 8 for the various radius ratios considered. The Ra-ranges at which the pseudo-conduction regime was found are plotted using full lines. Obviously, the transitional Ra increases with R. The variations of $\overline{Nu}$ against Ra obtained through increases in Ra beyond the

Table 3
Comparison of transitional Rayleigh numbers

R	1	1.04	1.08	1,12	1.16	1.20	$\sqrt{2}$	1.60
Present results		1735	1770	1810	1870	1915	–	–
Kim and Ro (1994)		–	–	–	–	1920	2150	2355
Correlation (10)	1702	1728	1774	1820	1866	1912	2158	2372

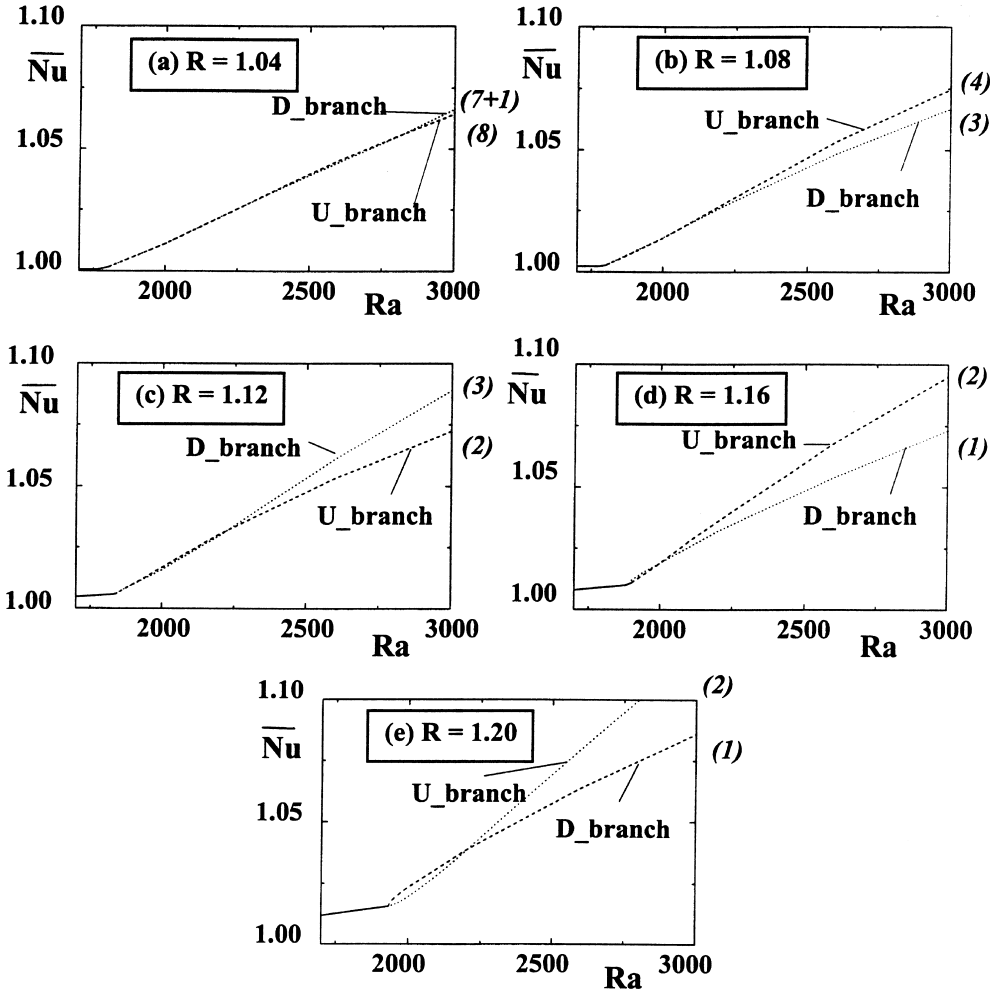

Fig. 8. Bifurcation diagrams of the mean Nusselt number for various radius ratios (Pr = 0.71).

threshold are plotted using dashed lines. For $R \leqslant 1.16$, these $\overline{Nu}$-values are located on the U-branch while they are on the D-branch for $R = 1.20$. A possible reason for this change is that this radius ratio is close to the threshold between 2D and 3D flows which can develop after the first transition, as it has been experimentally shown by Powe et al. (1969). The isolated $\overline{Nu}$-curves obtained by using the second procedure (abrupt increase in Ra from a perturbed pseudo-conduction solution up to 3000) are plotted using doted lines. It can be seen that the $\overline{Nu}$-values calculated are smaller or higher than those obtained with the first procedure, the branch where the Nusselt number is the highest being for the largest number of cells. Increase in the cell number leads indeed to an increase of the convective heat transfer between the cylinders. It is also seen that the two branches deviate from each other all the more since R is large because there are only one or two cells for $R \geqslant 1.16$.

At $Ra = 3000$ all the cells are counter-rotating, except for $R = 1.04$. At this radius ratio, seven cells are counter-rotating and one cell is co-rotating with the base flow when the solution is on the D-branch. The eight cells are counter-rotating on the U-branch. It should be noted that Fig. 2 shown in Kim and Ro (1994) and the present Fig. 8 for $R = 1.20$ are very similar. However, Kim and Ro found $Ra_c = 2330$ instead of 1915. At slightly higher Ra, they obtained an abrupt transition towards a multicellular flow having four secondary cells (two in each half-annulus) instead of the two cells that we have found just above the transitional Ra. When decreasing Ra and by starting their computations from the solution calculated at $Ra = 3000$, they obtained a second critical Rayleigh number equal to 1935, i.e. very near to the one determined in the present work (Table 3). Nevertheless, the change in the slopes of the branches shown in Fig. 2 of Kim and Ro (1994) at $Ra = 1935$ suggests a change in the flow structure that Kim and Ro have not mentioned.

Although large discrepancies are found amongst the results reported in the literature quoted in the reference section, the present results are not fully opposite. Only two types of steady multicellular flows were indeed reported in these works: the flow patterns are systematically characterized by the direction of velocity at $\theta = \pi$, upward or downward, or by the direction of the thermal plume, reversed or not. On the other hand, it is not the number of cells, which characterizes the nature of the flow as it was often assumed. The different numbers of cells as well as the discrepancies in Ra_c (Powe et al., 1969; Rao et al., 1985; Kim and Ro, 1994; Cheddadi et al., 1992) are probably due to uses of inappropriate convergence criteria and/or coarse grid resolutions (Fant et al., 1989; Kim and Ro, 1994).

A final comment regarding the recent paper by Yoo (1998), which pertains to the subject of the present work is in order. Yoo discretized the streamfunction-vorticity formulation of the Navier–Stokes equations using very fine meshes, i.e. (15×257) or (25×129) within half-annulus. For a radius ratio $R = 1.167$ he found the same behavior of the thermal cells as in the present study. For a low Prandtl number fluid (Pr = 0.3),

he determined a transitional value of the Rayleigh number equal to 2100. The present Eq. (10) gives $Ra_T = 1894$ for this radius ratio but for $Pr = 0.7$. This shows that there is only a weak effect of the Prandtl number on the onset of the steady multicellular motion at the annulus top. Moreover, the same kind of instabilities, thermal in their origin, were found to appear first. Two branches were also determined which are characterized by the direction of the fluid in the centered plane (ascending or descending). He remarked that once the thermal plume on the top has been established, its orientation (downward or upward) is not varied by increasing or decreasing Ra.

3.2. Flow patterns at moderate Rayleigh numbers

A second type of instability, hydrodynamic in its origin, was simulated at moderate Rayleigh numbers, i.e. for Ra values less than 50 000. All the subsequent calculations were carried out on the whole annulus ($0 \leqslant \theta \leqslant 2\pi$) using a uniform 31×240 grid system.

Fig. 9 shows the streamlines for various Ra and for a radius ratio $R = 1.14$. At $Ra = 9000$ instabilities are still thermal in origin. One may observe four stationary counter-rotating cells at the upper part of the annulus. When increasing Ra up to 15 000, oscillatory flow patterns appear within the main crescent-shaped cells. These hydrodynamic instabilities take the form of longitudinal rolls often observed in a vertical slot. As a consequence, the cells at the upper part of the annulus start to oscillate, changing their sizes alternatively and regularly. Low amplitude characterizes this periodic motion so that the dissymmetry of the flow structure is weak. At $Ra = 25\,000$, a chaotic motion appears. By increasing further Ra, the rolls within the main cells merge and a reverse transition to a unicellular main cell-structure is obtained at $Ra = 30\,000$ (Fig. 9d). The oscillatory behavior of the upper cells was already mentioned by Rao et al. (1985). In their study on flows in annulus filled with very low Prandtl number, Fant et al. (1989,1990) found also that amplification of hydrodynamic instabilities leads to roll formations within the main cells. Contrarily to what has been found for a vertical slot in which the hydrodynamic cells are stationary, the present calculations show that the secondary instabilities are unsteady, the internal cells within the vertical portion of the annulus drifting downward. This phenomenon can be compared to the unsteadiness which appears in the slot when surface radiation is accounted for (Desrayaud and Lauriat, 1988) or in the vertical annulus (Le Quéré and Pécheux, 1989). In both cases, the loss of symmetry of the base flow is the reason for unsteady instabilities.

Fig. 9. Streamlines for various Ra-values ($R = 1.14$, $Pr = 0.71$).

Once again, our results are in close agreement with those of Yoo (1998) who has shown for $Pr = 0.3$ that secondary hydrodynamic instabilities occur in the vertical section of the annulus, rendering the flow unsteady with the development of multiple oscillatory cells having a strong time periodic motion and drifting downward. On the other hand, the shape and strength of the thermal cells at the annulus top were almost unvarying.

4. Conclusions

A literature survey of natural convection within horizontal annuli of small radius ratios indicates the presence of multiplicity of solutions. On the other hand, the results discussed in the present paper reveal the existence of an imperfect bifurcation: there are only two stable branches of bifurcation, and thus only two modes of solutions. The mechanisms of formation or merging of the cells within the upper part of the annulus are indeed the same on the two branches, the number of cells depending mainly on the radius ratio and the Rayleigh number. For a fixed supercritical value of the Rayleigh number, the number of cells increases as the radius ratio decreases. When $R \to 1$ the number of cell tends toward infinity and the classical Rayleigh–Bénard problem characterized by a pitchfork bifurcation is recovered.

The reason for the large discrepancies in critical values and hysteresis phenomena found in the literature is probably due to the use of inappropriate criteria for stopping the calculations, too coarse grids or too large time steps.

The multicellular flows calculated in the present study undergo an unsteady secondary instability when increasing the Rayleigh number provided the radius ratio is small enough (for example $R = 1.14$). At moderate Ra, the resulting periodic flow is composed of cellular patterns within the base flow. This second type of instability is hydrodynamic in its origin. Like in air-filled vertical slots, a reverse transition to unicellular base flow is observed when increasing the Rayleigh number.

Acknowledgements

The authors are grateful for the support of the Picardie region (pôle modélisation) and the "Institut du Développement et des Ressources en Informatique Scientifique" (IDRIS) through projects No. 970714 and 981030.

References

Barbosa Mota, J.P., Saatdjian, E., 1994. Natural convection in a porous horizontal cylindrical annulus. J. Heat Transfer 116, 621–626.

Bergé, P., Pomeau, Y., Vidal, Ch., 1984. In: Hermann (Ed.), L'ordre dans le chaos.

Cadiou, P., 1997. Contribution à l'étude numérique des transferts de chaleur par convection naturelle ou par convection mixte dans une cavité annulaire horizontale. Ph.D. thesis, University of Marne-la-Vallée.

Cadiou, P., Lauriat, G., Mojtabi, A., 1995. A numerical solution for bifurcative natural convection in air-filled horizontal annuli of

small radius ratio. In: Bilgen, E., Mir, A., (Eds.), Proceedings of the Third International Thermal Energy Congress, vol. 1, pp. 397–403.

Cheddadi, A., Caltagirone, J.P., Mojtabi A, , Vafai, K., 1992. Two-dimensional convective bifurcation in a horizontal annulus. J. Heat Transfer 114, 99–106.

Desrayaud, G., Lauriat, G., 1988. Radiative influence on the stability of fluids enclosed in vertical cavities. Int. J. Heat Mass Transfer 31, 1035–1048.

Desrayaud, G., Lauriat, G., 1991. On the difficulties in computing bifurcation points: application to buoyant plumes In: Durand, M., El Dabaghi (Eds.), High Performance Computing II, North Holland, Amsterdam, pp. 609–621.

Fant, D.B., Rothmayer, A., Prusa, J., 1989. Natural Convective Flow Instability Between Horizontal Concentric Cylinders. Pineridge Press, Swansea, UK, vol. 6, No. (2), pp. 1047–1065.

Fant, D.B., Prusa, J., Rothmayer, A., 1990. Unsteady multicellular natural convection in a narrow horizontal cylindrical annulus. J. Heat Transfer 112, 379–387.

Kim, C.J., Ro, S.T., 1994. Numerical investigation on bifurcative natural convection in an air-filled horizontal annulus. In: Hewitt G.F. (Ed.), Proceedings of the 10th International Heat Transfer Conference, Brighton, vol. 7, pp. 85–90.

Lee, Y., Korpela, S.A., 1983. Multicellular natural convection in a vertical slot. J. Fluid Mech. 126, 91–121.

Quéré, P., Pécheux, J., 1989. Numerical simulations of multiple flow transitions in axisymmetric annulus convection. J. Fluid Mech. 206, 517–544.

Magnaud, J.P., Grand, D., Villand, M., Rouzaud, P., Hoffmann, A., 1997. International Topical Meeting on Advances in Reactors Physics, Mathematics and Computation, p. 3.

Powe, R.E., Carley, C.T., Bishop, E.H., 1969. Free convective flow patterns in cylindrical annuli. J. Heat Transfer 91, 310–314.

Powe, R.E., Carley, C.T., Carruth, S.L., 1971. A numerical solution for natural convection in cylindrical annuli. J. Heat Transfer 93, 210–220.

Rao, Y., Miki, Y., Fukuda, K., Takata, Y., Hasegawa, S., 1985. Flow patterns of natural convection in horizontal cylindrical annuli. Int. J. Heat Mass Transfer 28, 705–714.

Yoo, J.S., 1998. Natural convection in a narrow horizontal cylindrical annulus: $Pr \leqslant 0.3$. Int. J. Heat Mass Transfer 41, 3055–3073.